


Iron chelation cancer therapy using hydrophilic block copolymers conjugated with deferoxamine

Kana Komoto^{1,2} | Takahiro Nomoto^{1,2} | Sjaikhurizal El Muttaqien^{1,2,3} |
Hiroyasu Takemoto^{1,2} | Makoto Matsui¹ | Yutaka Miura^{1,2} | Nobuhiro Nishiyama^{1,2,4} 

¹Laboratory for Chemistry and Life Science, Institute of Innovative Research, Tokyo Institute of Technology, Yokohama, Japan

²Department of Life Science and Technology, School of Life Science and Technology, Tokyo Institute of Technology, Yokohama, Japan

³Center for Pharmaceutical and Medical Technology, Agency for the Assessment and Application of Technology (BPPT), LAPTIAB I, PUSPIPTEK, Serpong, Indonesia

⁴Innovation Center of Nanomedicine (iCONM), Kawasaki Institute of Industrial Promotion, Kawasaki, Japan

Correspondence

Takahiro Nomoto and Nobuhiro Nishiyama, Laboratory for Chemistry and Life Science, Institute of Innovative Research, Tokyo Institute of Technology, 4259 Nagatsutacho, Midori-ku, Yokohama, Kanagawa 226-8503, Japan.

Emails: nomoto@res.titech.ac.jp (T.N.); nishiyama.n.ad@m.titech.ac.jp (N.N.)

Funding information

Ministry of Education, Culture, Sports, Science and Technology; Center of Innovation Program; Japan Society for the Promotion of Science, Grant/Award Number: 18K18383, 18H04163, 15H04635 and JPMJCE1305; Japan Agency for Medical Research and Development, Grant/Award Number: JP18am0301008 and JP18cm0106202

Abstract

Cancer cells have high iron requirements due to their rapid growth and proliferation. Iron depletion using iron chelators has a potential in cancer treatment. Previous studies have demonstrated that deferoxamine (DFO) specifically chelates Fe(III) and exhibited antitumor activity in clinical studies. However, its poor pharmacokinetics has limited the therapeutic potential and practical application. Although polymeric iron chelators have been developed to increase the blood retention, none of previous studies has demonstrated their potential in iron chelation cancer therapy. Here, we developed polymeric DFO by the covalent conjugation of DFO to poly(ethylene glycol)-poly(aspartic acid) (PEG-PAsp) block copolymers. The polymeric DFO exhibited iron-chelating ability comparable with free DFO, thereby arresting cell cycle and inducing apoptosis and antiproliferative activity. After intravenous administration, the polymeric DFO showed marked increase in blood retention and tumor accumulation in subcutaneous tumor models. Consequently, polymeric DFO showed significant suppression of the tumor growth compared with free DFO. This study reveals the first success of the design of polymeric DFO for enhancing iron chelation cancer therapy.

KEYWORDS

chelation, deferoxamine, drug delivery systems, iron, polymers

1 | INTRODUCTION

Iron is an essential nutrient for cell metabolisms including DNA synthesis and ATP production.¹ Cancer cells have high iron requirements due to their rapid growth and proliferation, and iron overload has been reported to promote oncogenesis and tumor

growth.^{1,2} In this context, iron depletion using iron chelators has been reported to inhibit cancer cell proliferation by inducing cell cycle arrest and apoptosis.³⁻⁶ In particular, deferoxamine (DFO), which is the widely used iron chelator for iron overload disease, has attracted much attention in cancer treatment because of the safety profiles approved by the US FDA. Due to its hexadentate

This is an open access article under the terms of the Creative Commons Attribution-NonCommercial License, which permits use, distribution and reproduction in any medium, provided the original work is properly cited and is not used for commercial purposes.

© 2020 The Authors. *Cancer Science* published by John Wiley & Sons Australia, Ltd on behalf of Japanese Cancer Association.

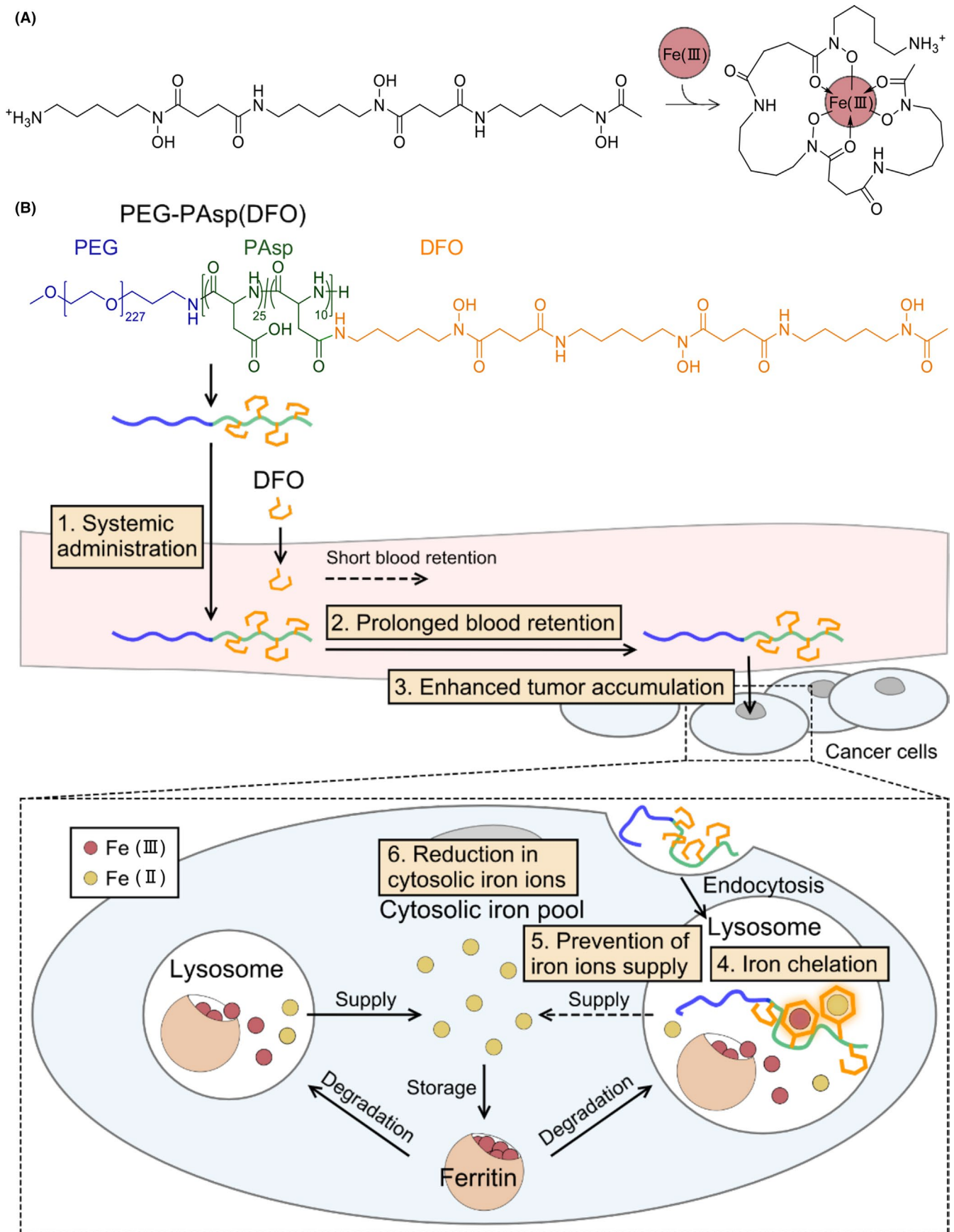


FIGURE 1 Expected effects of PEG-PAsp(DFO). A, Chemical structures of DFO and DFO/Fe(III). B, Chemical structure of PEG-PAsp(DFO) and its expected effects. Due to its high molecular weight, PEG-PAsp(DFO) should prolong blood retention and enhance tumor accumulation through the EPR effect, while DFO is quickly cleared from the bloodstream. In the tumor, PEG-PAsp(DFO) is expected to be endocytosed into cells and localized in lysosomes. As lysosomes are rich in iron ions because of degradation of Fe(III)-loaded ferritin and supply Fe(II) to the cytosol, PEG-PAsp(DFO) may chelate lysosomal Fe(III) and prevent release of Fe(II) to the cytosol, reducing the amount of metabolically active cytosolic Fe(II)

hydroxamates structure (Figure 1A), DFO specifically chelates Fe(III) with a log stability constant of 30, while it has a relatively low affinity to the other essential metals because of their divalent charge.^{7,8} In addition, the hexadentate ligand prevents Fe(III) from producing hydroxy radicals *via* Fenton reaction,^{7,9,10} which may contribute to avoidance of untoward toxicity. Previous studies have demonstrated that numerous cancer cell lines are sensitive to iron depletion by DFO.^{6,11-15} In addition, several clinical studies have shown that DFO exhibits antitumor activity in patients with neuroblastoma, leukemia, and hepatocellular carcinoma.¹⁶⁻¹⁸ However, DFO has an extremely short plasma half-life of approximately 20 min in human,⁷ limiting the therapeutic efficiency. To make up for such short blood retention, DFO must be infused for 8-24 h consecutively per day for several days per week,¹⁶⁻¹⁸ which may lead to arduous regimen for patients. In addition, systemically administered DFO cannot target tumors, and this may compromise its therapeutic potential.⁷ Overcoming these challenges may permit efficient iron chelation cancer therapy.

A promising way to increase the plasma half-life of DFO is covalently conjugating DFO to biocompatible polymers using its terminal amino group which does not contribute to iron chelation (Figure 1A).⁷ There has been extensive research in this field for iron overload diseases,¹⁹⁻²¹ in which polymeric DFO successfully increased the plasma half-life of DFO and resulted in enhancing the therapeutic effect. For iron chelation cancer therapy, due to prolonged blood retention, polymeric DFO has been expected to passively target tumors through an enhanced permeability and retention (EPR) effect.⁷ However, none of previous studies has reported the augmented antitumor activity of polymeric DFO and quantitatively evaluated its tumor accumulation.^{22,23}

Here, to realize effective iron chelation cancer therapy, we synthesized the polymeric DFO, termed PEG-PAsp(DFO), by covalently conjugating DFO to poly(ethylene glycol)-poly(aspartic acid) (PEG-PAsp; Figure 1B, upper). Our previous studies have reported that PEG-poly(amino acid) block copolymers could be promising platforms for cancer treatment due to its prolonged blood retention and enhanced tumor accumulation with efficient intratumoral penetration.^{24,25} Thus, we used PEG-PAsp as a backbone of our polymeric DFO. In addition, PEG-PAsp(DFO) could be synthesized with a narrow molecular weight distribution which may be useful as a model of polymeric DFO to investigate the pharmacokinetics. We studied the iron-chelating ability and antiproliferative activity in cultured cancer cells and examined its biodistribution and tumor growth suppression effect in subcutaneous tumor models. Our results indicated that intravenously injected PEG-PAsp(DFO) exhibited significantly prolonged blood circulation and enhanced tumor accumulation compared with free DFO. After internalization *via* endocytosis, PEG-PAsp(DFO) could chelate lysosomal Fe(III), which is believed

to come from ferritin that is degraded in lysosomes to supply Fe(II) to cytosolic iron pool. Eventually by inhibiting the supply of Fe(II), PEG-PAsp(DFO) decreased cytosolic Fe(II) levels. This chelation ultimately led to the antiproliferative effect in cultured cancer cells and the augmented suppression of the tumor growth compared with free DFO in a subcutaneous tumor model. To the best of our knowledge, this is the first report to demonstrate the advantages of polymeric iron chelators in cancer treatment.

2 | MATERIALS AND METHODS

2.1 | Materials

Materials are described in Doc S1.

2.2 | Cell lines and animals

DLD-1 cells and CT26 cells were purchased from the American Type Culture Collection (Manassas, VA). DLD-1 cells and CT26 cells were cultured in RPMI 1640 medium supplemented with 10% FBS and 1% penicillin/streptomycin under a humidified atmosphere containing 5% CO₂ at 37°C. BALB/c and BALB/c nu/nu mice (female, 4 wk old) were purchased from Charles River Laboratories Japan, Inc (Yokohama, Japan). All animal experiments were approved by the Animal Care and Use Committee of Tokyo Institute of Technology and performed in accordance with the Guidelines for the Care and Use of Laboratory Animals as stated by the Tokyo Institute of Technology.

2.3 | Synthesis of PEG-PAsp(DFO)

PEG-PAsp was synthesized as previously reported (Doc S1).²⁶ DFO was conjugated to PEG-PAsp by condensation reaction of the primary amino group of DFO and the carboxyl group of PEG-PAsp. The detailed methods on synthesis and characterization are described in Doc S1.

2.4 | Colorimetric analysis of iron-chelating ability

DFO and PEG-PAsp(DFO) (DFO concentration = 0.313 mmol/L, 80 μ L) in D-PBS(-) were mixed with FeCl₃ (1.25 mmol/L, 20 μ L, 1.00 eq to DFO) in D-PBS(-), respectively. Absorption spectrum was measured using an absorptiometer (NanoDrop One, Thermo Fisher Scientific, Inc).

2.5 | Flow cytometric analysis of intracellular iron ions

DLD-1 cells were seeded in 24-well plates (5.0×10^4 cells/well) and incubated at 37°C overnight. The cells were treated with samples (DFO concentration = 200 $\mu\text{mol/L}$) for 24 h. After incubation, the cells were washed with D-PBS(-) and incubated with 0.1 $\mu\text{mol/L}$ calcein-AM for 30 min. The cells were washed with D-PBS(-) and the fluorescence intensities of calcein were measured using a flow cytometer (Guava easy-Cyte 6-2 L, Merck Millipore, Billerica, MA).

2.6 | Microscopic imaging of intracellular Fe(II)

Details are described in Doc S1.

2.7 | Fluorometric analysis of intracellular Fe(II)

Details are described in Doc S1.

2.8 | Subcellular distribution

DLD-1 cells were seeded in 35 mm² glass base dishes (5.0×10^4 cells/dish) and incubated at 37°C overnight. The cells were treated with samples (DFO concentration = 200 $\mu\text{mol/L}$) for 24 h. After incubation, the cells were washed with D-PBS(-) and incubated with 100 nmol/L LysoTracker Red DND-99 for 30 min. The cells were washed with D-PBS(-) and incubated with 16 $\mu\text{mol/L}$ Hoechst 33342 stain for 5 min. The cells were washed with D-PBS(-) and observed in medium using a confocal laser scanning microscope (LSM710, Carl Zeiss Co., Ltd., Oberkochen, Germany).

2.9 | Cellular uptake

DLD-1 cells were seeded in 75 mm² flasks (5.0×10^6 cells/flask) and incubated at 37°C overnight. The cells were treated with Ga(III)-coordinated samples (DFO concentration = 200 $\mu\text{mol/L}$; the preparation method is described in Doc S1) for 24 h. After incubation, the cells were washed with D-PBS(-), harvested, and counted. The cells were then ashed with 200 μL of 70% HNO₃. The ashed samples were diluted to 2.0 mL with water. Ga concentration was measured using an inductively coupled plasma-mass spectrometry (Agilent 7900 ICP-MS, Agilent Technology Co., Ltd., Santa Clara, CA). Cellular uptake was calculated using the following equation:

$$\begin{aligned} & \text{Cellular uptake}(\% \text{Ga}/\text{cell}) \\ &= (\text{internalized Ga}) / (\text{dosed Ga}) \times 100 / \text{cell number}, \end{aligned}$$

where *internalized Ga* is the Ga content in the investigated sample, and *dosed Ga* is the Ga content in the treatment solution.

2.10 | Antiproliferative activity

Antiproliferative activity was examined using a Cell Counting Kit-8 (CCK-8), following the manufacturer's instruction. Briefly, DLD-1 cells were seeded in 96-well plates (1.0×10^3 cells/well) and incubated at 37°C overnight. Cells were treated with samples at various concentrations for 72 h. After incubation, the cells were incubated with CCK-8 solution for 2 h. Absorbances at 450 nm were measured using a microplate reader (iMark Microplate Reader, Bio-Rad, Hercules, CA).

2.11 | Cell cycle analysis

DLD-1 cells were seeded into 6-well plates (1.0×10^5 cells/well) and incubated at 37°C overnight. The cells were treated with samples at respective IC₅₀ for 72 h. After incubation, the cells were harvested and fixed in 70% ethanol overnight at -20°C. The cells were washed with D-PBS(-) and incubated with staining solution containing 10 $\mu\text{g/mL}$ propidium iodide (PI) and 100 $\mu\text{g/mL}$ RNase A for 30 min. The fluorescence intensities of PI were measured using Guava easy-Cyte 6-2 L.

2.12 | Flow cytometric analysis of DNA synthesis

Details are described in Doc S1.

2.13 | Microscopic imaging of DNA synthesis

Details are described in Doc S1.

2.14 | Apoptosis assay

Apoptosis assay was carried out using Apoptosis Kit, following the manufacturer's instruction. DLD-1 cells were seeded into 6-well plates (1.0×10^5 cells/well) and incubated at 37°C overnight. The cells were treated with samples (DFO concentration = 100 $\mu\text{mol/L}$) for 24 h. After incubation, the cells were washed with D-PBS(-) and incubated with staining solution containing FITC-annexin V and PI for 15 min. The fluorescence intensities of FITC and PI were measured using Guava easy-Cyte 6-2 L.

2.15 | Biodistribution study

Female 5-wk-old BALB/c mice were inoculated subcutaneously with CT26 cells (1.0×10^5 cells/mouse). The tumor size was measured using an electronic caliper, and the tumor volume (V) was calculated using the following equation:

$$V = a \times b^2 / 2,$$

where a and b are the major and minor axes of the tumor, respectively. When the average tumor volume reached around 200 mm^3 , Ga(III)-coordinated samples (the preparation method is described in Doc S1) were intravenously injected into the tail vein ($1.52 \text{ } \mu\text{mol DFO/mouse}$). Mice were sacrificed 1, 3, 6 and 24 h after intravenous injection, and blood, organs, and tumors were collected and weighed. The samples were then ashed with 1.0 mL of $70\% \text{ HNO}_3$. The ashed samples were diluted to 10 mL with water. Ga concentration was measured using Agilent 7900 ICP-MS.

2.16 | Tumor growth suppression

Antitumor activity of free DFO and PEG-PAsp(DFO) was examined using BALB/c nu/nu mice bearing subcutaneous DLD-1 tumors and BALB/c mice bearing subcutaneous CT26 tumors. Female 5-wk-old BALB/c nu/nu and BALB/c mice were subcutaneously inoculated with DLD-1 cells (1.0×10^6 cells/mouse) and CT26 cells (1.0×10^5 cells/mouse), respectively. When the average tumor volume reached around 100 mm^3 , DFO or PEG-PAsp(DFO) was intravenously injected into the tail vein ($1.52 \text{ } \mu\text{mol DFO/mouse}$).

2.17 | Blood test and histological analysis

Details are described in Doc S1.

3 | RESULTS

3.1 | Synthesis of PEG-PAsp(DFO)

PEG-PAsp(DFO) was synthesized by simple conjugation of DFO to the PAsp segment of the hydrophilic PEG-PAsp (Figure 1B; M_n of PEG: $10\,000$; polymerization degree of PAsp: 35) (the synthetic scheme is shown in Figure S1). The introduction number of DFO to PAsp side chain was determined to be 10 using $^1\text{H NMR}$ spectroscopy (Figure S2). Although the amide formation of DFO should decrease its water solubility,²⁷ the PEG-PAsp offered excellent hydrophilicity and PEG-PAsp(DFO) showed a narrow molecular weight distribution in aqueous solution without distinctive aggregates, which was confirmed by gel permeation chromatography (Figure S3).

3.2 | Iron-chelating properties

To elucidate iron-chelating ability of PEG-PAsp(DFO), the absorption spectra of free DFO and PEG-PAsp(DFO) were measured in the absence or presence of Fe(III). It is known that sole Fe(III) has an absorbance peak around 270 nm while the complex of DFO and Fe(III) (DFO/Fe(III)) exhibits a characteristic absorption peak around

430 nm .^{28,29} Indeed, as shown in Figure 2A, free DFO/Fe(III) revealed the peak around 430 nm , whereas free DFO itself did not have this characteristic peak. Importantly, the mixture of PEG-PAsp(DFO) and Fe(III) (PEG-PAsp(DFO)/Fe(III)) also exhibited the peak around 430 nm , and the absorption spectrum was considerably similar to DFO/Fe(III), suggesting that PEG-PAsp(DFO) possessed iron-chelating ability comparable with free DFO.

We also examined intracellular iron-chelating ability of PEG-PAsp(DFO) by calcein method, an established method to evaluate a level of intracellular iron ions.³⁰⁻³² Although fluorescent calcein is widely used for the analysis of Ca(II), it also forms a complex with cytosolic iron ions and quenches the fluorescence. The decrease in the number of cytosolic iron ions prevents this complex formation, leading to enhancement of the fluorescence intensity of calcein. Thus, the fluorescence intensity of calcein inversely correlates with a level of cytosolic iron ions. Figure 2B shows the calcein fluorescence of cells treated with free DFO or PEG-PAsp(DFO). Both free DFO and PEG-PAsp(DFO) significantly increased calcein fluorescence, indicating considerable chelation of cytosolic iron ions.

Note that the calcein method cannot clearly distinguish Fe(II) and Fe(III) while recent studies reported the preferential complex formation of calcein with Fe(III).³³ To get more insight into the chelation effect of free DFO and PEG-PAsp(DFO), we observed intracellular Fe(II) using confocal laser scanning microscopy (CLSM) using FerroOrange, which emits strong fluorescence upon reaction with Fe(II) (Figure 2C). Free DFO and PEG-PAsp(DFO) significantly decreased FerroOrange fluorescence. The decreased fluorescence intensity was further confirmed by quantitative fluorometric analysis (Figure 2D). Although DFO specifically chelated Fe(III) with high stability, these results suggested that free DFO and PEG-PAsp(DFO) decreased intracellular Fe(II) level.

3.3 | Subcellular distribution and cellular uptake

To examine subcellular distribution of PEG-PAsp(DFO), DLD-1 cells were incubated with Cy5-labeled PEG-PAsp(DFO) (Cy5-PEG-PAsp(DFO)) for 24 h and observed using CLSM (Figure 3A). Cy5-PEG-PAsp(DFO) was localized in endo-/lysosomes, suggesting that Cy5-PEG-PAsp(DFO) should be taken up through endocytic pathway. Next, cellular uptake of DFO in PEG-PAsp(DFO) was compared with that of free DFO. As DFO forms stable complex with Ga(III) with high stability constants second to Fe(III),³⁴⁻³⁶ we used Ga-coordinated DFO (DFO/Ga(III)) and PEG-PAsp(DFO) (PEG-PAsp(DFO)/Ga(III)) to quantify the cellular uptake. DLD-1 cells were incubated with DFO/Ga(III) or PEG-PAsp(DFO)/Ga(III) for 24 h and the amount of intracellular Ga was quantified using inductively coupled plasma-mass spectroscopy (ICP-MS; Figure 3B). PEG-PAsp(DFO)/Ga(III) exhibited less cellular uptake than DFO/Ga(III). This might be due to a steric hindrance conferred by PEG that inhibits interaction with the surface of cancer cells.³⁷

FIGURE 2 Iron-chelating ability. A, Absorption spectra in the presence or absence of Fe(III) in D-PBS(-). B, Flow cytometric analysis of intracellular iron ions using calcein-AM. DLD-1 cells were incubated with samples for 24 h. The results are expressed as means \pm SD ($n = 4$). Statistical significance was evaluated using Tukey's multiple comparison test. **** $P < .0001$. C, CLSM imaging of intracellular Fe(II) using FerroOrange. DLD-1 cells were incubated with samples for 24 h. Yellow: Intracellular Fe(II) (FerroOrange). D, Fluorometric analysis of intracellular Fe(II) using FerroOrange. DLD-1 cells were incubated with samples for 24 h. The results are expressed as means \pm SD ($n = 5$). Statistical significance was evaluated using Tukey multiple comparison test. **** $P < .0001$

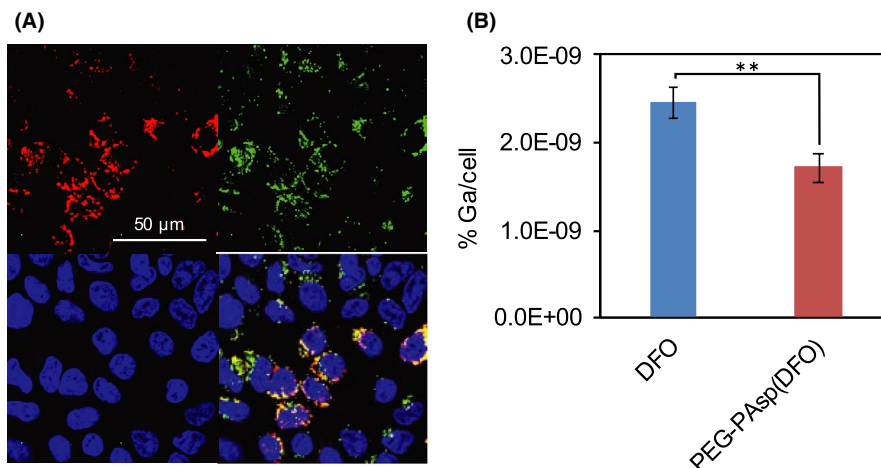
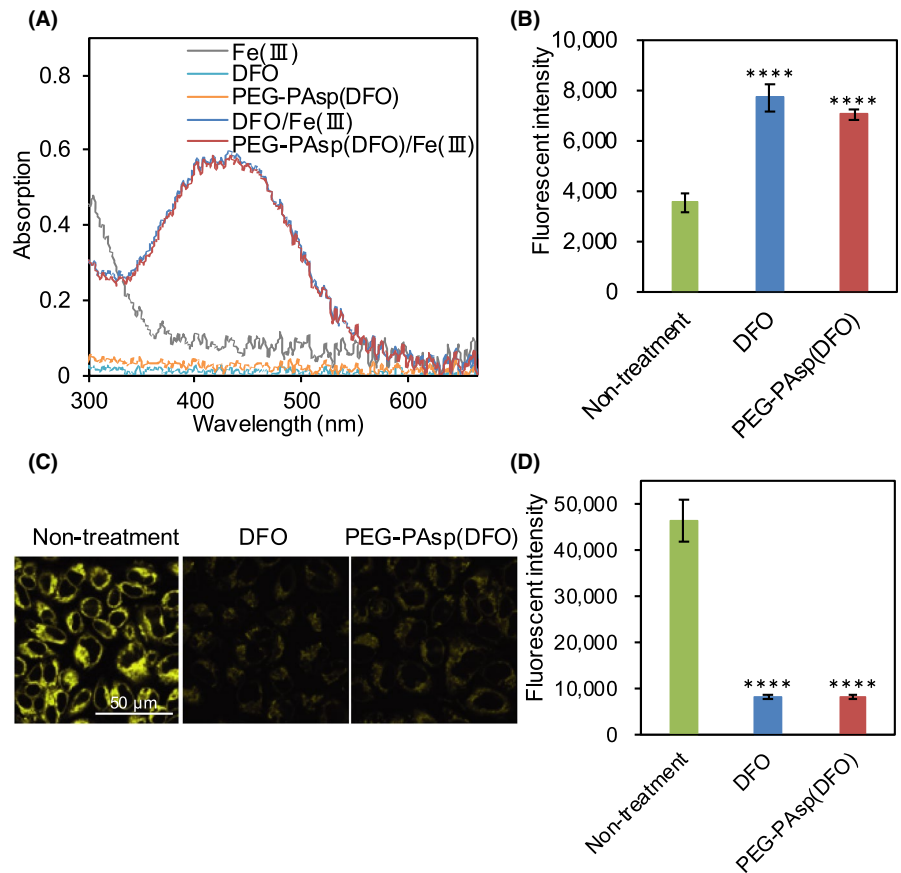


FIGURE 3 Subcellular distribution and cellular uptake. A, Subcellular distribution. Cells were incubated with Cy5-PEG-PAsp(DFO) for 24 h. Subcellular distribution was imaged using CLSM. Red: Cy5-PEG-PAsp(DFO); green: endo-/lysosomes (LysoTracker Red DND-99); blue: nuclei (Hoechst 33342). B, Cellular uptake. Cells were treated with DFO/Ga(III) or PEG-PAsp(DFO)/Ga(III) for 24 h. The amount of cellular Ga uptake was quantified using ICP-MS. The cellular uptake (%Ga/cell) is defined as (internalized Ga)/(dosed Ga) \times 100/ cell number. The results are expressed as means \pm SD ($n = 3$). Statistical significance was evaluated using Student t test. ** $P < .01$

3.4 | Antiproliferative activity

We next examined antiproliferative activity of free DFO and PEG-PAsp(DFO) (Figure 4). Free DFO clearly inhibited cell proliferation even in the low concentration region ($<10 \mu$ M), which is consistent with the previous reports.^{3,11-15} PEG-PAsp(DFO)

also exhibited antiproliferative activity in a dose-dependent manner. IC_{50} values of free DFO and PEG-PAsp(DFO) were 3.5 and 20 μ M/L (DFO equivalent), respectively. This relatively low antiproliferative activity of PEG-PAsp(DFO) might be due in part to the less cellular uptake compared with free DFO (Figure 3B).

Iron chelators have been reported to inhibit cancer proliferation by inducing cell cycle arrest and apoptosis.³⁻⁶ To explore the antiproliferative mechanisms of PEG-PAsp(DFO), we first analyzed cell cycle of cells treated with free DFO and PEG-PAsp(DFO) at IC₅₀ doses (Figure 5). Free DFO and PEG-PAsp(DFO) increased the S phase fraction from 16.2% of non-treatment group to 60.4% and 58.0%, respectively. This result suggested that free DFO and PEG-PAsp(DFO) arrested the cell cycle at S phase. As iron is an essential component of enzymes that are responsible for DNA synthesis,^{38,39} this S phase arrest might be attributed to inhibition of DNA synthesis. Thus, we analyzed DNA synthesis inhibition using BrdU. Immunofluorescence staining revealed that free DFO and PEG-PAsp(DFO) inhibited the incorporation of BrdU (Figure 6A). This was further confirmed by CLSM observation, in which free DFO and PEG-PAsp(DFO) decreased the number of cells exhibiting a punctate BrdU staining pattern (Figure 6B). This inhibition of DNA synthesis may contribute to the S phase arrest.

To further examine antiproliferative mechanisms, the apoptosis fraction was quantified using FITC-annexin V and PI (Figure 7). Free DFO and PEG-PAsp(DFO) exhibited significantly higher fraction of early apoptotic cells, achieving 31.0% and 37.9%, than the non-treatment group (10.7%). A slight increase of late apoptotic and necrotic cells fractions was also observed in free DFO and PEG-PAsp(DFO) (3.31% and 3.95%, respectively) compared with the non-treatment group (1.58%). In summary, PEG-PAsp(DFO) induced S phase arrest by inhibiting DNA synthesis and caused cell apoptosis, thereby exhibiting the antiproliferative effect.

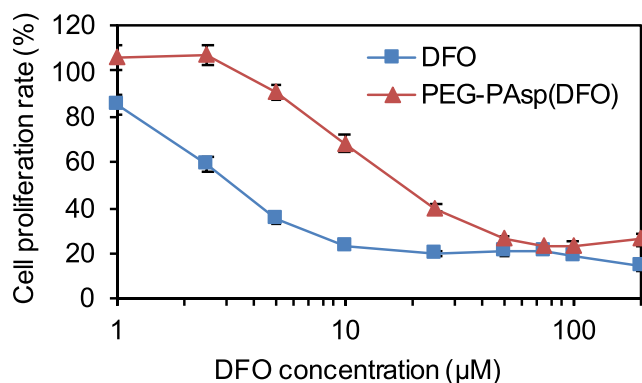


FIGURE 4 Antiproliferative activity. DLD-1 cells were incubated with samples at various concentrations for 72 h. Cell proliferation was analyzed using CCK-8. The results are expressed as means \pm SD (n = 5)

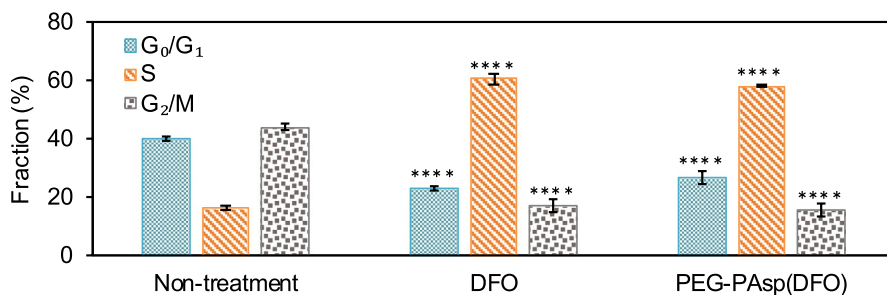


FIGURE 5 Cell cycle analysis using flow cytometry with PI. DLD-1 cells were treated with samples at respective IC₅₀ for 72 h. Results are expressed as means \pm SD (n = 3). Statistical significance was evaluated using Tukey multiple comparison test. ****P < .0001

3.5 | Biodistribution study

To examine biodistribution, we intravenously injected DFO/Ga(III) or PEG-PAsp(DFO)/Ga(III) into mice bearing subcutaneous CT26 tumors and quantified the amount of Ga in the tissues using ICP-MS (Figures 8 and S4). Consistent with previous studies,^{7,40} DFO/Ga(III) was rapidly cleared from blood, revealing 0.25% dose/mL 1 h after injection (Figure 8A). Free DFO/Ga(III) should be excreted through the kidneys where its high accumulation was observed (Figure S4A). By contrast, PEG-PAsp(DFO)/Ga(III) showed drastically prolonged retention in blood, achieving >10% dose/mL 6 h after injection (Figure 8A), which can be explained by the high molecular weight of the polymer.

As iron ions in blood dominantly exist as transferrin-loaded form and DFO cannot chelate these iron ions,⁴¹ enhancing intertumoral concentration of DFO must be key to efficient iron chelation cancer therapy. Regarding tumor accumulation (Figure 8B), DFO/Ga(III) exhibited only a 0.13% dose/g tumor 6 h after injection due to its rapid clearance from the body. By contrast, PEG-PAsp(DFO)/Ga(III) efficiently accumulated in tumor tissue and gradually increased the level, achieving 3.9% dose/g tumor 6 h after injection, which corresponds to 30 times higher level than DFO/Ga(III). Additionally, PEG-PAsp(DFO)/Ga(III) maintained high concentration in tumor tissue even 24 h after injection, revealing 1.99% dose/g tumor. This augmented tumor accumulation could be explained by the EPR effect.

3.6 | Tumor growth suppression and safety studies

Finally, antitumor activity of PEG-PAsp(DFO) was examined using mice bearing subcutaneous DLD-1 tumors (Figure 9A,B). PEG-PAsp(DFO) significantly suppressed tumor growth compared with free DFO (P = .043 on day 16). No obvious weight loss was observed in the treatment period, suggesting that free DFO and PEG-PAsp(DFO) did not cause severe side effects. A similar result was also obtained for subcutaneous CT26 tumor models (Figure 9C,D). In addition, we investigated the possible effects of PEG-PAsp(DFO) on the kidneys where its high accumulation was observed (Figure S4B); no significant differences were observed in the levels of BUN, CRE, and uric acid (Table S1), suggesting that PEG-PAsp(DFO), as well as free DFO, did not induce apparent damage to the kidneys. The safety of PEG-PAsp(DFO) was further confirmed by histological analysis of the kidney (Figure S5).

FIGURE 6 Analysis of DNA synthesis using BrdU and FITC BrdU antibodies. A, Flow cytometric analysis. DLD-1 cells were treated with samples at respective IC_{50} for 72 h. B, CLSM imaging. DLD-1 cells were incubated with samples at respective IC_{50} for 72 h. Red: BrdU (FITC anti-BrdU antibodies); blue: nuclei (Hoechst 33342)

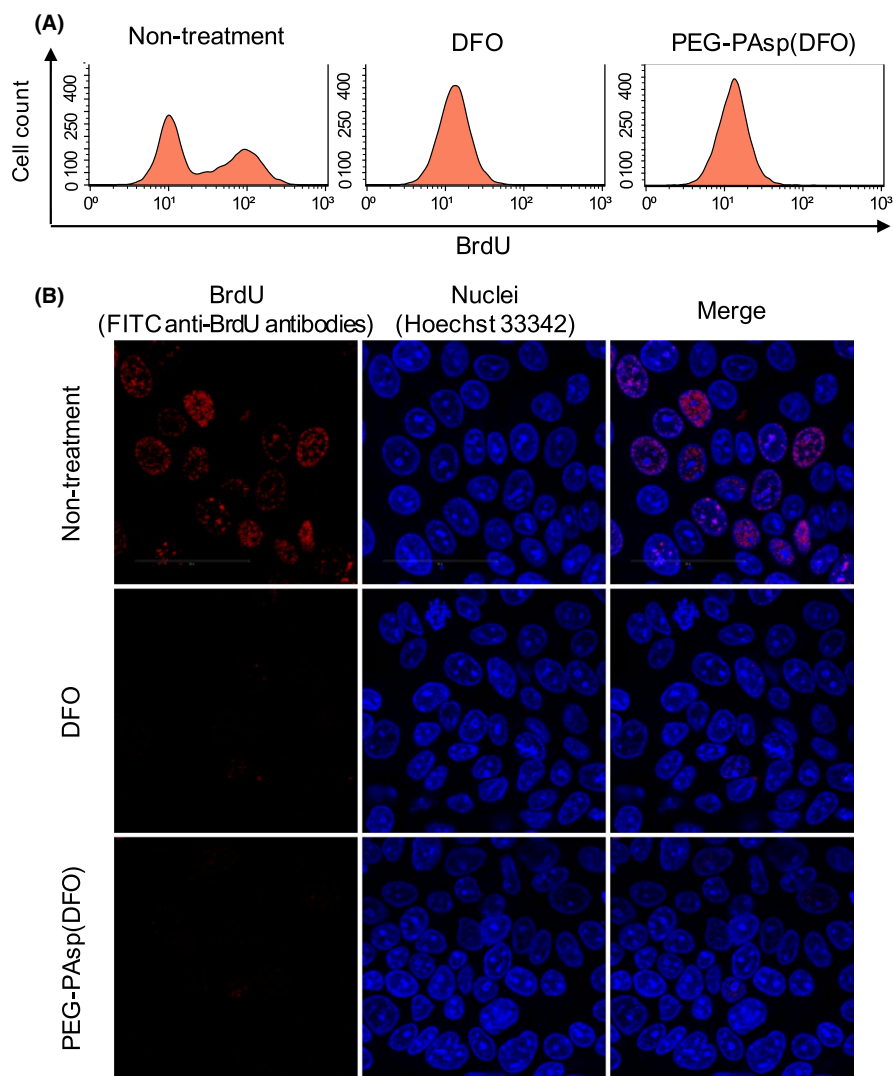
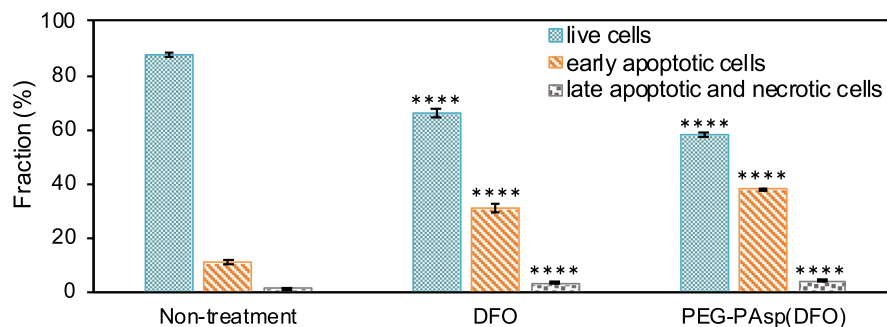


FIGURE 7 Apoptosis analysis using flow cytometry with FITC-annexin V and PI. DLD-1 cells were treated with samples (DFO concentration = 100 μ mol/L) for 24 h. Results are expressed as means \pm SD ($n = 3$). Statistical significance was evaluated using Tukey multiple comparison test. **** $P < .0001$



4 | DISCUSSION

Many previous studies reported that iron deprivation has a great potential in cancer treatment in *in vitro* conditions,^{6,11-15} and DFO has been most extensively investigated as the efficient iron chelator because of its excellent iron-selectivity and safety.^{7,10} However, only a few studies have demonstrated its *in vivo* therapeutic efficiency probably due to its poor biodistribution. To overcome the short blood retention, Kemp et al and Blatt et al investigated the potential of polymeric iron chelator, hydroxyethyl starch conjugated-DFO

(HES-DFO).^{22,23} Despite the fact that HES-DFO has successfully increased the blood retention,^{21,22,42} HES-DFO alone failed to inhibit the tumor growth, and its tumor accumulation level remains to be clarified. Hence, this study investigated the physicochemical properties, *in vitro* activity, pharmacokinetics, and antitumor effect of our polymeric iron chelator, PEG-PAsp(DFO).

Regarding the iron-chelating activity of free DFO and PEG-PAsp(DFO), they may have chelated both of intracellular and extracellular iron ions because they increased the antiproliferative effect after their DFO concentration exceeded the iron

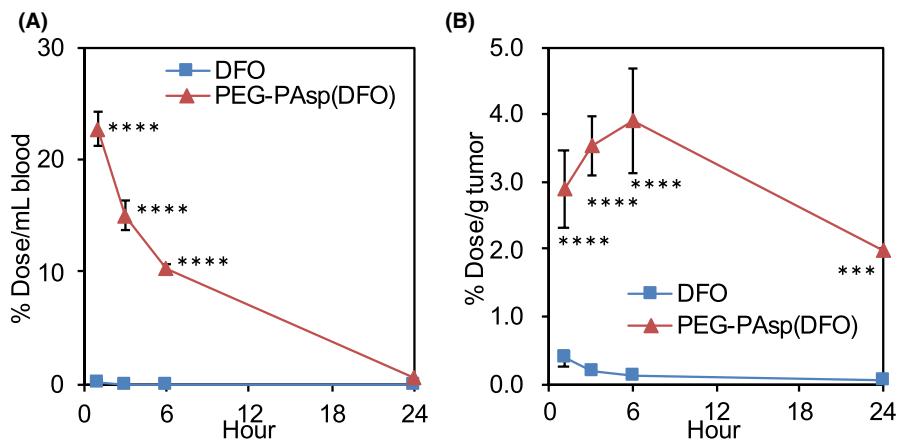


FIGURE 8 Biodistribution. A, B, DFO/Ga(III) or PEG-PAsp(DFO)/Ga(III) was intravenously injected into the mouse bearing subcutaneous CT26 tumors, and the concentration of Ga in (A) blood and (B) tumors was quantified by measuring Ga concentration using ICP-MS. Results are expressed as means \pm SD ($n = 3$). Statistical significance was evaluated using Tukey multiple comparison test. **** $P < .0001$

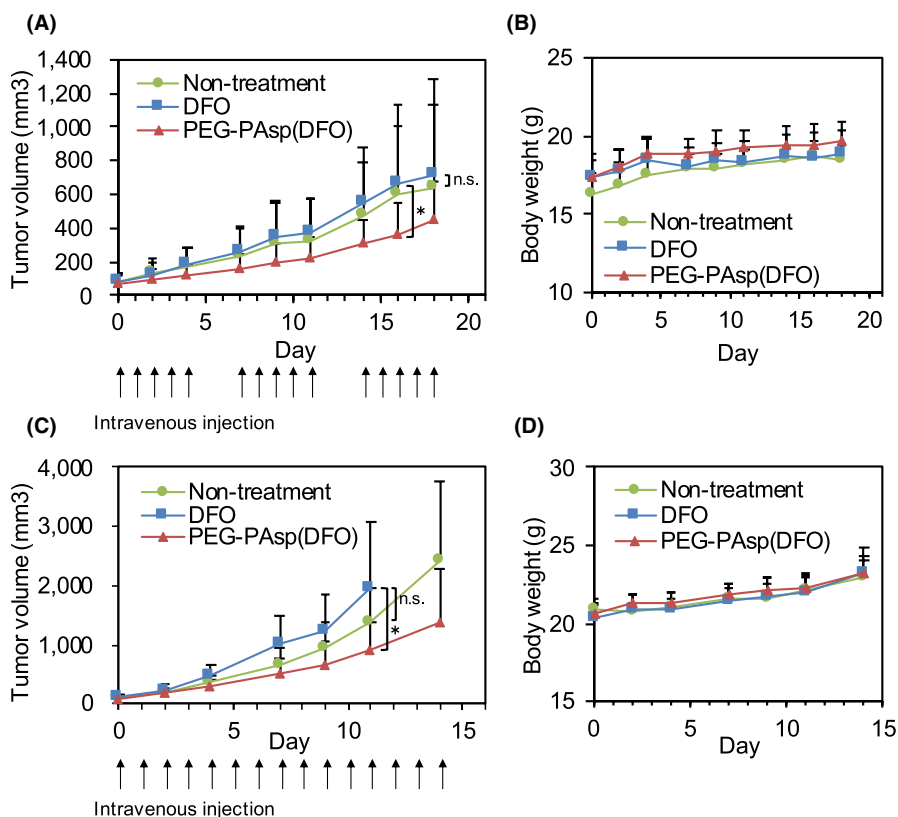


FIGURE 9 Tumor growth suppression. A, B, (A) Tumor volume and (B) body weight in subcutaneous DLD-1 tumor models. Samples were injected intravenously into the mouse 5 times a week ($1.52 \mu\text{mol DFO/mouse}$). The results are expressed as means \pm SD (non-treatment: $n = 7$; DFO: $n = 8$; PEG-PAsp(DFO): $n = 8$). Statistical significance was evaluated using Tukey's multiple comparison test. * $P < .05$. C, D, (C) Tumor volume and (D) body weight in subcutaneous CT26 tumor models. Samples were intravenously injected into the mouse every day for 15 d ($1.52 \mu\text{mol DFO/mouse}$). The results are expressed as means \pm SD (non-treatment: $n = 6$; DFO: $n = 8$; PEG-PAsp(DFO): $n = 6$). Statistical significance was evaluated using Student *t* test. * $P < .05$

ions concentration in the medium ($\sim 3 \mu\text{M}$; Figure 4). Free DFO and PEG-PAsp(DFO) should first chelate extracellular iron ions, and their intracellular chelation might critically affect cell viability. Indeed, DFO is believed to be taken up through endocytosis due to its poor membrane permeability, and exerts its activity by chelating iron ions mainly in endo-/lysosomes.⁴³ As CLSM observation revealed that PEG-PAsp(DFO) was localized in endo-/lysosomes (Figure 3A), PEG-PAsp(DFO) might also chelate endo-/lysosomal iron ions. Although free DFO and PEG-PAsp(DFO) might chelate iron ions in endo-/lysosomes, they efficiently decreased the cytosolic iron ions level (Figure 2B). These interesting phenomena may be explained by prevention of iron ions supply from ferritin. Lysosomes are rich in iron ions because iron-loaded ferritin is degraded in lysosomes to supply iron ions into cytosolic

iron pool⁴⁴⁻⁴⁶; and DFO localization in lysosomes has been demonstrated to stimulate ferritin degradation,^{45,47} probably because lysosomal iron chelation by DFO might prevent the iron ions supply. PEG-PAsp(DFO) in the lysosome might also prevent this supply, thereby lowering the cytosolic iron level as illustrated in Figure 1B. Note that iron in the endo-/lysosomes is likely to be Fe(II) due to the acidic and reducing environment.⁴⁶ Regardless of the preferential chelation of DFO with Fe(III), PEG-PAsp(DFO) and free DFO significantly decreased intracellular Fe(II) levels (Figure 2C,D). It is possible that they might chelate the iron ions that are transiently oxidized to Fe(III). Another possibility is that they might chelate Fe(II) as well as Fe(III) to some extent, while their affinity to Fe(II) is much lower than Fe(III). These possible activities might reduce intracellular Fe(II).

By chelating intracellular iron ions, PEG-PAsp(DFO) induced S phase arrest (Figure 5). It has been reported that major cellular iron requirements occur during late G₁ and S phases^{5,48} due in part to the increased activity of ribonucleotide reductase, which requires iron to catalyze a rate-limiting step of DNA synthesis.^{38,39} Iron depletion could suppress the activity of this enzyme^{40,49} and inhibit DNA synthesis, which might lead to S phase arrest. In line with these observations, our results provided compelling evidence that PEG-PAsp(DFO) inhibited DNA synthesis (Figure 6). Note that iron deprivation has been reported to arrest the cell cycle at G₁ and G₂/M phases as well as S phase.^{3,48,50} It has been inferred that there are multiple stages that are sensitive to iron deprivation, and cellular responses should be dependent on experimental conditions.^{50,51} Consistent with the previous studies, when we treated DLD-1 cells with 100 μmol/L free DFO for 48 h, it arrested cells at the G₁ phase (Figure S6). Meanwhile, similar treatment with PEG-PAsp(DFO) resulted in S phase arrest. However, precise mechanisms underlying these differences remain unclear; further investigation is still needed.

Despite the difference in dose dependency in cell cycle arrest, both iron chelators induced apoptosis with the similar efficiency (Figure 7). Apoptosis induction in this study might be explained by the iron-dependent functions of hypoxia inducible factor 1α (HIF1α) and p53. That is, iron deprivation has been reported to stabilize HIF1α by inhibiting prolyl hydroxylases, which require iron to regulate HIF1α protein level.¹ The stabilized HIF1α may increase the p53 level,^{52,53} thereby inducing cell apoptosis. Furthermore, a previous study has demonstrated that the cell cycle arrest should be dependent on the level of p53; the normal level should lead to G₁ phase arrest, while the low level may result in S phase arrest.⁵⁴ Thus, we will investigate the role of p53 in the biological activity of PEG-PAsp(DFO) in a future study.

Although free DFO exhibited marked in vitro antiproliferative activity as demonstrated in Figure 4, free DFO disappeared rapidly from the blood and did not show the antitumor effect (Figures 8 and 9). By contrast, PEG-PAsp(DFO) showed significantly prolonged retention in blood, and the DFO concentration in blood 1 h after injection (approximately 0.35 mmol/L) clearly surpassed the reported concentration of non-transferrin-bound iron in blood (<5.0 μmol/L).^{55,56} Most importantly, PEG-PAsp(DFO) accomplished significantly enhanced tumor accumulation at 3.9% dose/g tumor (~100 μmol/L DFO) 6 h after injection. This tumor accumulation level corresponded to the concentration for >70% growth inhibition in the cultured cells (Figure 4). Conversely, free DFO reached only 2.0 μmol/L in the tumor, at which concentration only 30% cell growth inhibition was observed (Figure 4). In good agreement with the biodistribution, PEG-PAsp(DFO) significantly suppressed the tumor growth compared with free DFO (Figure 8A,C). Thus, our results indicated the consistency between the biodistribution and pharmacodynamics of the iron chelators in cancer treatment. The efficacy of iron chelation cancer therapy could be markedly enhanced by polymeric DFO. It should be noted that a considerable amount of PEG-PAsp(DFO) accumulated in the kidney (Figure S4B), however, no apparent acute toxicity could

be observed (Table S1; Figure S5); this may be partially because DFO-coordinated iron ion does not participate in the Fenton reaction.^{7,9,10} This minimal toxicity would offer great promise in a therapy that combines iron chelation and anticancer drugs, as the iron chelation is also reported to inhibit the expression of stemness markers of cancer stem cells.⁵⁷

ACKNOWLEDGMENTS

We thank the Division of Materials Analysis Suzukake-dai, Technical Department, Tokyo Institute of Technology. This work was supported by the Center of Innovation program from the Japan Science and Technology Agency, Basic Science and Platform Technology Program for Innovative Biological Medicine (JP18am0301008) from Japan Agency for Medical Research and Development (AMED), the Project for Cancer Research And Therapeutic Evolution (P-CREATE) (JP18cm0106202) from AMED, JSPS KAKENHI Grant Numbers 18K18383, 18H04163, 15H04635, and Five-star Alliance from the Ministry of Education, Culture, Sports, Science and Technology (MEXT).

DISCLOSURE

The authors declare no conflict of interest.

ETHICAL CONSIDERATIONS

All animal experiments were approved by the Animal Care and Use Committee of Tokyo Institute of Technology and performed in accordance with the Guidelines for the Care and Use of Laboratory Animals as stated by the Tokyo Institute of Technology.

ORCID

Nobuhiro Nishiyama  <https://orcid.org/0000-0002-6886-9357>

REFERENCES

1. Torti SV, Torti FM. Iron and cancer: more ore to be mined. *Nat Rev Cancer*. 2013;13(2):342-355.
2. Hann HWL, Stahlhut MW, Menduke H. Iron enhances tumor growth. *Cancer*. 1991;68:2407-2410.
3. Harima H, Kaino S, Takami T, et al. Deferasirox, a novel oral iron chelator, shows antiproliferative activity against pancreatic cancer in vitro and in vivo. *BMC Cancer*. 2016;16(1):702.
4. Kovar J, Valenta T, Stybrova H. Differing sensitivity of tumor cells to apoptosis induced by iron deprivation in vitro. *Vitr Cell Dev Biol*. 2001;37(7):450-458.
5. Kulp KS, Green SL, Vulliet PR. Iron deprivation inhibits cyclin-dependent kinase activity and decreases cyclin D/CDK4 protein levels in asynchronous MDA-MB-453 human breast cancer cells. *Exp Cell Res*. 1996;229(1):60-68.
6. Yang Y, Xu Y, Su A, Yang D, Zhang X. Effects of deferoxamine on leukemia in vitro and its related mechanism. *Med Sci Monit*. 2018;24:6735-6741.
7. Hamilton JL, Kizhakkedathu JN. Polymeric nanocarriers for the treatment of systemic iron overload. *Mol Cell Ther*. 2015;3(1):3.
8. Hernlem BJ, Vane LM, Sayles GD. Stability constants for complexes of the siderophore desferrioxamine b with selected heavy metal cations. *Inorganica Chim Acta*. 1996;244(2):179-184.
9. Graf E, Mahoney JR, Bryant RG, Eaton JW. Iron-catalyzed hydroxyl radical formation. *J Biol Chem*. 1984;259(6):3620-3624.

10. Bogdan AR, Miyazawa M, Hashimoto K, Tsuji Y. Regulators of iron homeostasis: new players in metabolism, cell death, and disease. *Trends Biochem Sci*. 2016;41(3):274-286.
11. Chaston TB, Lovejoy DB, Watts RN, Richardson DR. Examination of the antiproliferative activity of iron chelators: multiple cellular targets and the different mechanism of action of triapine compared with Deferrioxamine and the Potent Pyridoxal Isonicotinoyl Hydrazone Analogue 311. *Clin Cancer Res*. 2003;9:402-414.
12. Bajbouj K, Shafarin J, Hamad M. High-dose deferoxamine treatment disrupts intracellular iron homeostasis, reduces growth, and induces apoptosis in metastatic and nonmetastatic breast cancer cell lines. *Technol Cancer Res Treat*. 2018;17:1-11.
13. Becton DL, Bryles P. Deferoxamine inhibition of human neuroblastoma viability and proliferation. *Cancer Res*. 1988;48:7189-7192.
14. Seligman PA, Schleicher RB, Siriwardana G, Domenico J, Gelfand EW. Effects of agents that inhibit cellular iron incorporation on bladder cancer cell proliferation. *Blood*. 1993;82(5):1608-1617.
15. Blatt J, Taylor SR, Kontoghiorghes GJ. Comparison of activity of deferoxamine with that of oral iron chelators against human neuroblastoma cell lines. *Cancer Res*. 1989;49(11):2925-2927.
16. Yamasaki T, Terai S, Sakaida I. Deferoxamine for advanced hepatocellular carcinoma. *N Engl J Med*. 2011;365(6):576-578.
17. Donfrancesco A, Deb G, Dominici C, Pileggi D, Castello MA, Helson L. Effects of a single course of deferoxamine in neuroblastoma patients. *Cancer Res*. 1990;50(16):4929-4930.
18. Estrov BZ, Tawa A, Wang X-H, et al. In vitro and In vivo effects of deferoxamine in neonatal acute leukemia. *Blood*. 1987;69(3):757-761.
19. Imran Ul-Haq M, Hamilton JL, Lai BFL, et al. Design of long circulating nontoxic dendritic polymers for the removal of iron in vivo. *ACS Nano*. 2013;7(12):10704-10716.
20. Wang Y, Liu Z, Lin TM, Chanana S, Xiong MP. Nanogel-DFO conjugates as a model to investigate pharmacokinetics, biodistribution, and iron chelation in vivo. *Int J Pharm*. 2018;538(1-2):79-86.
21. Hamilton JL, Imran ul-haq M, Abbina S, et al. In vivo efficacy, toxicity and biodistribution of ultra-long circulating desferrioxamine based polymeric iron chelator. *Biomaterials*. 2016;102:58-71.
22. Kemp JD, Cardillo T, Kehrberg E, et al. Inhibition of lymphoma growth in vivo by combined treatment with hydroxyethyl starch deferoxamine conjugate and IgG monoclonal antibodies against the transferrin receptor. *Cancer Res*. 1995;55(17):3817-3824.
23. Blatt J, Boegel F, Hedlund BE, Arena VC, Shaddock RK. Failure to alter the course of acute myelogenous leukemia in the rat with subcutaneous deferoxamine. *Leukemia Res*. 1991;15(5):391-394.
24. Mi P, Yanagie H, Dewi N, et al. Block copolymer-boron cluster conjugate for effective boron neutron capture therapy of solid tumors. *J Control Release*. 2017;254:1-9.
25. Nomoto T, Nishiyama N. Design of drug delivery systems for physical energy-induced chemical surgery. *Biomaterials*. 2018;178:583-596.
26. Koide A, Kishimura A, Osada K, Jang WD, Yamasaki Y, Kataoka K. Semipermeable polymer vesicle (PICsome) self-assembled in aqueous medium from a pair of oppositely charged block copolymers: Physiologically stable micro-/nanocapsules of water-soluble macromolecules. *J Am Chem Soc*. 2006;128(18):5988-5989.
27. Aaseth J, Crisponi G, Andersen O. *Chelation Therapy in the Treatment of Metal Intoxication*. Amsterdam, Netherlands: Academic Press, Elsevier; 2016.
28. Goodwin JF, Whitten CF. Chelation of ferrous sulphate solutions by desferrioxamine. *Nature*. 1965;16(4968):281-283.
29. Liu Z, Lin TM, Purro M, Xiong MP. Enzymatically biodegradable polyrotaxane-deferoxamine conjugates for iron chelation. *ACS Appl Mater Interfaces*. 2016;8(39):25788-25797.
30. New EJ. Tools to study distinct metal pools in biology. *Dalt Trans*. 2013;42(9):3210-3219.
31. Prus E, Fibach E. Flow cytometry measurement of the labile iron pool in human hematopoietic cells. *Cytom Part A*. 2008;73(1):22-27.
32. Tenopoulou M, Kurz T, Doulias PT, Galaris D, Brunk UT. Does the calcein-AM method assay the total cellular 'labile iron pool' or only a fraction of it? *Biochem J*. 2007;403(2):261-266.
33. Thomas F, Serratrice G, Béguin C, et al. Calcein as a fluorescent probe for ferric iron. Application to iron nutrition in plant cells. *J Biol Chem*. 1999;274(19):13375-13383.
34. Evers A, Hancock RD, Martell AE, Motekaitis RJ. Metal ion recognition in ligands with negatively charged oxygen donor groups: complexation of Fe(III), Ga(III), In(III), Al(III), and other highly charged metal ions. *Inorg Chem*. 1989;28(11):2189-2195.
35. Borgias B, Hugi AD, Raymond KN. Isomerization and solution structures of desferrioxamine B complexes of Al³⁺ and Ga³⁺. *Inorg Chem*. 1989;28(18):3538-3545.
36. Wang S, Lee RJ, Mathias CJ, Green MA, Low PS. Synthesis, purification, and tumor cell uptake of ⁶⁷Ga-deferoxamine-folate, a potential radiopharmaceutical for tumor imaging. *Bioconjug Chem*. 2002;7(1):56-62.
37. Hatakeyama H, Akita H, Harashima H. The polyethyleneglycol dilemma: advantage and disadvantage of PEGylation of liposomes for systemic genes and nucleic acids delivery to tumors. *Biol Pharm Bull*. 2013;36(6):892-899.
38. Björklund S, Skogman E, Thelander L. An S-phase specific release from a transcriptional block regulates the expression of mouse ribonucleotide reductase R2 subunit. *EMBO J*. 1992;11(13):4953-4959.
39. Erikssons S, Graslund A, Skog S, Thelander L, Tribukait B. Cell cycle-dependent regulation of mammalian ribonucleotide reductase. *J Biol Chem*. 1984;259(19):11695-11700.
40. Chenoufi N, Baffet G, Drénou B, et al. Deferoxamine arrests in vitro the proliferation of porcine hepatocyte in G1 phase of the cell cycle. *Liver*. 2008;18(1):60-66.
41. Hallberg L, Hedenberg L. The effect of deferoxamine on iron metabolism in man. *Scand J Haematol*. 1965;2:67-79.
42. Hallaway PE, Eaton JW, Panter SS, Hedlund BE. Modulation of deferoxamine toxicity and clearance by covalent attachment to biocompatible polymers. *Proc Natl Acad Sci USA*. 1989;86(24):10108-10112.
43. Doulias PT, Christoforidis S, Brunk UT, Galaris D. Endosomal and lysosomal effects of desferrioxamine: protection of HeLa cells from hydrogen peroxide-induced DNA damage and induction of cell-cycle arrest. *Free Radic Biol Med*. 2003;35(7):719-728.
44. Terman A, Kurz T. Lysosomal iron, iron chelation, and cell death. *Antioxid Redox Signal*. 2013;18(8):888-898.
45. Kidane TZ, Sauble E, Linder MC. Release of iron from ferritin requires lysosomal activity. *Am J Physiol Physiol*. 2006;291(3):445-455.
46. Kurz T, Eaton JW, Brunk UT. The role of lysosomes in iron metabolism and recycling. *Int J Biochem Cell Biol*. 2011;43(12):1686-1697.
47. De DI, Ward DM, Kaplan J. Specific iron chelators determine the route of ferritin degradation. *Blood*. 2009;114(20):4546-4551.
48. Nurtjahja-Tjendraputra E, Fu D, Phang JM, Richardson DR. Iron chelation regulates cyclin D1 expression via the proteasome: a link to iron deficiency-mediated growth suppression. *Blood*. 2007;109(9):4045-4054.
49. Green DA, Antholine WE, Wong SJ, Richardson DR, Chitambar CR. Inhibition of malignant cell growth by 311, a novel iron chelator of the pyridoxal isonicotinoyl hydrazone class. *Clin Cancer Res*. 2001;7(11):3574-3579.
50. Renton FJ, Jeitner TM. Cell cycle-dependent inhibition of the proliferation of human neural tumor cell lines by iron chelators. *Biochem Pharmacol*. 1996;51(11):1553-1561.
51. Fukuchi K, Tomoyasu S, Watanabe H, et al. G1 accumulation caused by iron deprivation with deferoxamine does not accompany change of pRB status in ML-1 cells. *Biochim Biophys Acta*. 1997;1357:297-305.
52. An WG, Kanekal M, Simon MC, Maltepe E, Blagosklonny MV, Neckers LM. Stabilization of wild-type p53 by hypoxia-inducible factor 1 α . *Nature*. 1998;392:7416-7419.

53. Graeber TG, Peterson JF, Tsai M, Monica K, Fornace AJ, Giaccia AJ. Hypoxia induces accumulation of p53 protein, but activation of a G1-phase checkpoint by low-oxygen conditions is independent of p53 status. *Mol Cell Biol.* 2012;14(9):6264-6277.
54. Agarwal ML, Agarwal A, Taylor WR, Chernova O, Sharma Y, Stark GR. A p53-dependent S-phase checkpoint helps to protect cells from DNA damage in response to starvation for pyrimidine nucleotides. *Proc Natl Acad Sci USA.* 1998;95(25):14775-14780.
55. Chua ACG, Olynyk JK, Leedman PJ, Trinder D. Non-transferrin bound iron uptake by hepatocytes is increased in a Hfe knockout mouse model of hereditary hemochromatosis. *Blood.* 2004;124(5):1519-1525.
56. Chansiw N, Pangjit K, Phisalaphong C, et al. Effect of a novel oral active iron chelator: 1-(N-acetyl-6-aminohexyl)-3-hydroxy-2-methylpyridin-4-one (CM1) in iron-overloaded and non-overloaded mice. *Asian Pac J Trop Med.* 2014;7(S1):155-161.
57. Ninomiya T, Ohara T, Noma K, Katsura Y. Iron depletion is a novel therapeutic strategy to target cancer stem cells. *Oncotarget.* 2017;8(58):98405-98416.

SUPPORTING INFORMATION

Additional supporting information may be found online in the Supporting Information section.

How to cite this article: Komoto K, Nomoto T, El Muttaqien S, et al. Iron chelation cancer therapy using hydrophilic block copolymers conjugated with deferoxamine. *Cancer Sci.* 2021;112:410-421. <https://doi.org/10.1111/cas.14607>